Molecular Mechanisms of Interphase Evolution in the Liquid Polystyrene−Glassy Poly(phenylene oxide) System

J. Pablo Tomba,*,† José M. Carella,† and José M. Pastor‡

Institute of Materials Science and Technology (INTEMA), National Research Council (CONICET), National University of Mar del Plata, Juan B. Justo 4302, (7600) Mar del Plata, Argentina, and Department of Physics of Condensed Matter, University of Valladolid, Paseo del Cauce s/n, (47011) Valladolid, Spain

Received January 2, 2009; Revised Manuscript Received April 1, 2009

ABSTRACT: We report a diffusion study on a series of interphases formed between a polystyrene-rich (PS) liquid layer and a poly(phenylene oxide) (PPO) glassy matrix. Diffusion was promoted by annealing the polymer pair at several temperatures below the glass transition temperature of the PPO matrix, in experiments where the liquid component was supplied from an *unlimited* source. Depth PS concentration profiles were obtained via optical sectioning through the glassy layer with confocal Raman microspectroscopy. The PS profiles measured in all the samples had sharp diffusion fronts followed by a region with relatively uniform PS concentration. From the time evolution of the PS front advance, we directly obtained the time-scaling laws for interphase kinetics which are interpreted in the context of the Fickean and case II diffusion theories. Despite some recent studies reporting the occurrence of case II in this particular system, our results and analysis show conclusively that interphase kinetics are, on the contrary, markedly Fickean. Results previously published by other authors on this polymer pair are also analyzed with the aim of offering a unified view about the mechanism that controls interphase evolution at the molecular level.

Introduction

Beyond its obvious importance in several technological fields, the diffusion of organic penetrants in glassy polymer matrices has been the focus of active research for many years. The penetration of *small* molecules, i.e., solvents, nonsolvents, and molecular dyes, into glassy polymers has been extensively studied, and the principles of this phenomenon are well understood. It has been well documented that, under certain conditions of temperature and concentration, penetration can be markedly non-Fickean, with some unique features labeled as case II diffusion. The application of ion-beam-based techniques by Kramer[1,2] has contributed to definitively understanding the foundations of this remarkable diffusion mechanism, confirming the ideas originally introduced by Thomas and Windle.[3] A more recent work by Argon updates some of the fundamentals, offering a more rigorous description of the driving forces involved in the process.[4]

Conventionally, studies of case II diffusion have been conducted by submerging a piece of the glassy polymer into an *infinite* source of small penetrant molecules; the theory around the phenomenon has also been developed under this condition. Driven by high levels of osmotic suction,[5] small molecules permeate through the surface of the glassy matrix filling first interstitial sites. The presence of small molecules creates a dilatational misfit and induces an effective (biaxial) stress field, mechanically counteracted by the constraint imposed by the glassy matrix. At a certain level of diluents, the induced stress field effectively overcomes the matrix yield stress and the glassy polymer is plastically deformed; this deformation rate controls further penetration of the small molecules, making it the rate-controlling step for the process. The condition of infinite supply of small molecules is not incidental as it guarantees a steady concentration of diluents driving the advance of the diffusion front. This whole set of conditions, i.e., high levels of osmotic suction, infinite supply of small molecules, and diffusion controlled by mechanical relaxation, give rise to the most recognizable case II feature: its linear diffusion kinetics.[3]

The penetration of *large*, mostly liquid, molecules in glassy polymer matrices has started to be considered much more recently. The criterion used here to distinguish between *small* and *large* penetrants is based on the inverse relationship existing between molecular size and osmotic suction;[5] while we consider as *small* molecules those that produce levels of osmotic suction in the range of the glassy matrix yield stress, *large* molecules are those that, under similar conditions, generate osmotic suctions far below this limit. Under this criterion, bulky plasticizers, oligomers and polymers are considered here as *large* molecules. The first experiments of diffusion of liquid polymer molecules in glassy matrices were reported by Kramer and Composto on the liquid polystyrene/glassy poly(phenylene oxide) (l-PS/g-PPO) polymer pair[6] and separately by Sauer and Peppas on the liquid poly(vinyl methyl ether)/glassy polystyrene (l-PVME/g-PS) system.[7,8] These studies emerged as cases of interdiffusion between two miscible polymers with different glass transition temperatures (T_g), conducted at temperatures intermediate between the T_gs of the components.

From a mechanistic point of view, the basis of the diffusion mechanisms involving large liquid molecules is not so well established as in the case of small-sized penetrants. Many authors brought the concepts learnt from case II to interpret the experimental evidence, i.e., liquid concentration profiles and apparent diffusion kinetics, implying that penetration of the liquid species are controlled by mechanical relaxation of the glassy polymer.[7,8] A different view offered by another group of authors describes the growing mechanism for these interphases as diffusion controlled, with characteristics similar to those observed in polymer diffusion in the melt state between species with different physical properties.[9,10] The extremely low osmotic suction associated with large-sized penetrants has been suggested as a factor that rules out case II diffusion in these systems.[9] Recent experiments on the l-PS/g-PPO and l-PVME/g-PS, carried out in the immediacy of T_g of the glassy polymer, have shown the absence of transition in the diffusion mode as

* To whom correspondence should be addressed. E-mail jptomba@fi.mdp.edu.ar.
† National University of Mar del Plata.
‡ University of Valladolid.

10.1021/ma802884j CCC: $40.75
Published on Web 04/22/2009

the PS passes from glassy to liquid state, which seems to support the latter view.[11] On the other hand, Lin and co-workers recently reported case II diffusion kinetics in experiments carried out on the l-PS/g-PPO system, with PS samples of moderate-to-high molecular weight, and at temperatures well below the T_g of PPO.[12]

A remarkable similarity between diffusion experiments involving large liquid molecules is that most of them have been conducted in settings of *limited* liquid supply, i.e., a thin liquid layer that diffuses in the glassy matrix, in opposition with the conventional *infinite* supply condition inherent to case II. In conditions of limited supply, under the constraint of mass conservation, the concentration of liquid polymer throughout this thin layer depletes with diffusion time. Therefore, the local material properties behind the advancing diffusion front change continuously while diffusion evolves, which sometimes misleads attempts to establish a connection between molecular mechanisms and apparent diffusion kinetics.[13]

This paper reports a diffusion study on a series of liquid/glassy polymer interphases, carried out under conditions of *unlimited* liquid polymer supply. We have chosen the l-PS/g-PPO system in part motivated by recent work that reports for the first time evidence of case II in this polymer pair. The idea of carrying out experiments in a setting of *unlimited* liquid polymer, with liquid molecular weights in the lower end, i.e., higher levels of osmotic suction, has been to reproduce as close as possible those conditions under which case II manifests unequivocally their distinctive features. As an experimental tool, we employed optical sectioning by confocal Raman microspectroscopy (CRM) in a configuration that delivers steady depth resolution, one order of magnitude improved with respect to that reported in our previous work. As the technique yields direct information on interphase concentration profiles, the results thus obtained can be straightforwardly analyzed in the context of Fickean and case II mechanisms. Results previously published by other authors for this polymer couple are also analyzed with the aim of offering a unified view about the dominating diffusion mechanism in these systems.

Time Scaling Laws for Polymer Diffusion Kinetics

We start with a brief overview on time scaling laws for diffusion kinetics in the context of the diffusion mechanisms relevant to this work. In the first stages of polymer diffusion between two melt phases, the chains close to the interface, subjected to entropic confinement, recover their Gaussian chain statistics that they lost because of the proximity to the interface. At these early stages, chain diffusion is non-Fickean and is characterized by complex time scaling laws.[14] As the diffusion distances spanned by this regime are typically below the radius of gyration of the chains, well beyond the detection limit of the experimental techniques considered here, we will not consider it in detail.

For longer distances, center-of-mass diffusion prevails. Driven by Brownian motion, polymer diffusion consists of random thermal jumps of segments of polymer chains between adjacent voids or free volume elements. The process is naturally described by Fick's law, through a transport (diffusion) coefficient D. The simplest case is tracer diffusion, i.e., a low concentration of polymer chains moving in an essentially invariant polymer matrix. For a given temperature, the process can be described by a single molecular weight (M) dependent diffusion coefficient, whose functionality with M can be expressed in terms of well-known regimes, i.e., Rouse, and reptation.[15] Concentration distributions of the diffusing species, mathematically described by combinations of error functions, have the characteristic sigmoidal shape. When diffusing species are present in appreciable amounts, thermodynamic factors start to operate (interdiffusion).[16] In the most general case, the diffusing polymer and the matrix have dissimilar segmental mobilities, i.e., different viscosity. This arises from differences in chemical structure, commonly manifested through differences in T_g, and from differences in molecular weight. In this case, the low-viscosity polymer diffuses through an environment progressively enriched in the component of high viscosity, experiencing a continuous, sometimes dramatic, drop in molecular mobility. Fick's law with a concentration-dependent diffusion coefficient describes well this experiment.[16] A bulk flow contribution has to be included to account for the asymmetric intrinsic diffusivity between components.[17] The distribution profiles predicted by these models, experimentally supported by many experiments, are highly asymmetric. In most of these cases, a sharp diffusion front, i.e., concentration dropping abruptly in a narrow spatial region, is observed, with the steeper slope in regions of lower molecular mobility (higher local T_g). A particular case is given when both liquid polymers are identical (self-diffusion); in this situation their molecular mobilities match, and a single diffusion coefficient describes the experiment.[16]

All the cases discussed above can be mathematically described by Fick's law. Focusing on the frequently studied one-dimensional diffusion case in planar geometry between two infinite layers, Fick's law predicts that the amount of substance passing through the original interface scales with time as $t^{1/2}$, with a slope inversely proportional to D; this relationship holds for constant or concentration-dependent D.[18] For the latter case, if a diffusion front develops, its advancing kinetics is also predicted to scale as $t^{1/2}$. Boundary conditions, source dimensions (limited or unlimited supply), and polydispersity in molecular weights may affect, to different extents, the apparent scaling laws for diffusion kinetics. In systems described by a single concentration-independent D, diffusion kinetics always scales as $t^{1/2}$, independently of the type of supply. In systems represented through concentration-dependent D, i.e., interdiffusion, the condition of limited supply (or finite source) may produce departures from the $t^{1/2}$ scaling. In the polymer couple, the constraint of mass conservation forces the concentration throughout the thinner layer to progressively decrease, thus changing local values of D and the slope of the Fickean plot.[19] A similar case is found in systems with polydispersity in molecular weights. At early stages, diffusion is dominated by the lower molecular weight species, ascribed to higher D values, while at longer diffusion times, center-of-mass transport of the higher molecular species prevails. Diffusion in polymer latex films exemplifies well this kind of behavior: the plots of mass fraction of diffused polymer as a function of $t^{1/2}$ usually show a downward curvature that reflects the decrease of D as the extent of diffusion increases.[20]

Several diffusion regimes have been described for diffusion of small molecules in glassy polymers, many of them Fickean, for which the above-mentioned scaling laws hold. Under certain conditions of penetrant activity and temperature, some systems manifest case II behavior.[3] In a typical experiment, a piece of glassy polymer is put in contact with an infinite source of gas or liquid penetrant. Over the induction period, penetration is essentially Fickean, described by a constant D.[1] Once conditions for control by case II are established, further transport of small penetrants in the glassy matrix occurs through a self-similar propagating front, with the Fickean precursor ahead.[4] The front is preceded by a plasticized layer with a nearly constant concentration of penetrant, which is continuously supplied by the infinite source. The resulting penetrant concentration profile is highly asymmetric due to the dramatic changes in molecular mobility experienced by the penetrant along its diffusion path. The advancing front kinetics has been modeled by a coupled

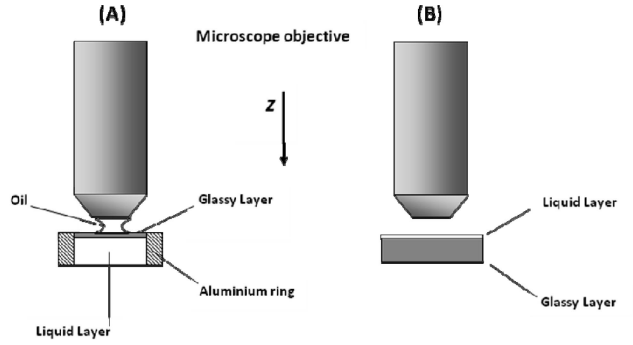

Figure 1. Schematic of the experimental setup used for optical sectioning by confocal Raman with (A) immersion optics and (B) dry optics.

Table 1. Characteristics of the Samples Used for Diffusion Experiments

	low-T_g layer		high-T_g layer	
system	Φ^{PS}	T_g [°C]	Φ^{PS}	T_g [°C]
l-PS0.7/g-PPO	0.7	25	0.05	200
l-PS1.5/g-PPO	0.9	51	0.1	182
l-PS3.9/g-PPO	0.9	80	0.1	185

nonlinear system of mass and momentum balance equations; a summary of the most relevant approaches can be found in ref 4. Under the assumption of constant (equilibrium) concentration of penetrant in the plasticized layer, the front is predicted to advance at constant velocity. A quantitative description of the effect of penetrant concentration in the plasticized layer on front velocity was first made by Hui[1] and has been recently revisited by Argon.[4] It is predicted that front velocities increase sharply with concentration of small molecules in the plasticized layer, particularly in the concentration range slightly above the critical value necessary for case II initiation. On the basis of those predictions, we anticipate that the type of supply ought to affect the apparent diffusion front kinetics: in experiments under limited liquid supply, as concentration of small molecules in the plasticized layer decreases, a downward deviation from the characteristic linear time scaling should be expected.

Experimental Section

Materials Characterization. Polystyrene (PS) samples were purchased from Polymer Source (Dorval, Canada), as materials with narrow molecular weight distributions ($M_w/M_n < 1.1$). Three PS samples having different molecular weights were employed, referred to here as PS0.7 (M_w = 740 g/mol, T_g = −5 °C), PS1.5 (M_w = 1460 g/mol, T_g = 45 °C), and PS3.9 (M_w = 3900 g/mol, T_g = 77 °C). The poly(phenylene oxide) (PPO) sample (M_n = 31 000 g/mol, M_w/M_n = 2.0, T_g = 212 °C) was purchased from Aldrich. The oil used as immersion fluid (B446082), with refractive index = 1.5, was purchased from Merck. Glass transition temperatures for pure polymers and their blends were measured by differential scanning calorimetry (DSC), with a Perkin-Elmer Pyris II DSC instrument. Samples were cooled and heated from −70 °C at rates of 10 °C/min under a N_2 atmosphere. T_gs were determined as the onset of the transition.

Sample Preparation for Diffusion Experiments. Details about samples for diffusion experiments can be found in Table 1. Cylindrical specimens (6.5 mm diameter) were prepared via sequential molding in a two-step process, carried out in a mold that operates under vacuum to avoid sample degradation. First, a thin film of the high-T_g PPO−PS blend, about 200 μm thick, was molded at 40 °C above its T_g. Next, an aluminum guard ring (see Figure 1) was placed and secured on top of that film, at room temperature. Finally, a thick layer of the low-T_g PPO−PS blend was vacuum-molded on top of the high-T_g blend layer, in the cavity formed by the aluminum guard ring. The temperature of the second molding step was set to about 30 °C above the respective blend T_g, to minimize diffusion between layers at this stage. To fulfill the condition of unlimited liquid supply, the liquid layer was about 5 times thicker than the glassy layer. These samples were annealed in a temperature-controlled oven (±0.5 °C) under a dry nitrogen atmosphere for a period of time. They were then removed from the oven and quickly cooled to room temperature, which virtually stops interphase evolution, to be microscopically characterized.

Confocal Raman Microspectroscopy. Local Raman spectra were measured at room temperature on a microspectrometer DILOR LabRam Confocal, equipped with a 16 mW He−Ne laser beam (632.8 nm wavelength). The pinhole opening (h) was set at 200 μm (h maximum is 1000 μm). In the excitation and collection path, an immersion Olympus x100 (numerical aperture, NA = 1.39) was the microscope objective primarily used. Some measurements were also carried out with a dry Olympus x100 (NA = 0.9) objective. A slit opening of 500 μm and a holographic grating of 1800 lines/mm were used to acquire Raman spectra in the shifts range between 500 and 1500 cm^{-1}, with a spectral resolution of about 4 cm^{-1}. The acquisition time for each spectrum varied between 2 and 5, and four spectra were accumulated for each data point.

Figure 1 shows two configurations for depth profiling by confocal Raman. Figure 1B shows that used in a major part of our previous work, which employs dry objectives. This configuration has the advantage of being noninvasive; i.e., the sample is scanned without contact, but at the cost of sacrificing spatial resolution.[11,21] With dry objectives, laser refraction at the air/sample interface distorts significantly the size of the laser spot, originally limited by diffraction, with the consequent worsening in depth discrimination.[22−24] At nominal focusing depths of 50 μm, predicted values of depth resolution are in the range 20−30 μm,[24] i.e., one order of magnitude larger than those predicted by diffraction theory. This deterioration in depth resolution is not steady and becomes more severe as one focuses deeper below the sample surface.[22] Another undesirable effect is that the depth scale is artificially compressed, making sample features to appear artificially closer to the microscope objective. Although this distortion can be corrected by rescaling the depth scale with a factor obtained from calculations based on geometric optics,[22] the broadening of sharp sample features due to the enlargement of the laser focal volume remains in the measurements.[25]

The configuration used in the present work overcomes those limitations by using immersion optics (Figure 1A). A coupling fluid between objective and sample that matches the sample refractive index is used to minimize laser deviation at the sample surface. In this way, the refraction influence is substantially reduced and depth resolution within the diffraction limits recovered. In order to adapt to operation with immersion optics, the glassy−liquid polymer interphase is now approached through the high-T_g solid layer, with the coupling oil on the external part of this layer, as shown in Figure 1A. Although PPO resisted well direct contact with the oil used here, we have proposed the use of a thin protective coating which can be reversibly applied onto the sample surface avoiding direct oil/sample contact and potential sample damage; details can be found elsewhere.[26] Notice that the initial thickness of the glassy layer was kept just below the working distance of the objective (210 μm), which allows us to see the original position of the glassy−liquid polymer interface and, at the same time, a wide span of depths to monitor interphase evolution inside the solid film. Overall, the method is expected to yield consistent depth resolution close to the diffraction limit and to completely suppress distortions of the depth scale.

For optical sectioning, diffusion specimens were mounted on a microscope stage with controlled vertical displacement (z-axis) coupled to the Raman spectrometer. A drop of coupling oil was placed between the glassy layer and the microscope objective just before confocal Raman profiling were carried out. The oil was exhaustively removed with tissue paper before sample annealing. Optical sections were obtained at various distances from the glassy layer surface by moving the focal plane along the z-direction (see Figure 1), resulting in a series of Raman spectra as a function of

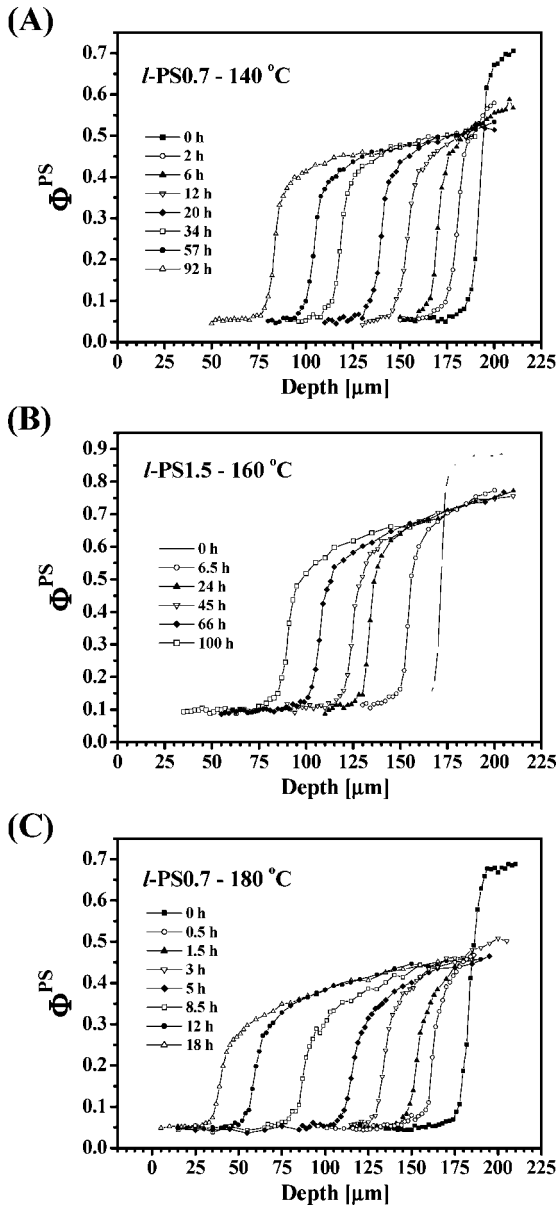

Figure 2. Typical PS concentration profiles obtained by confocal Raman depth profiling at l-PS/g-PPO interphases. Annealing times and temperatures and the type of PS sample are specified in the legends.

depth. The methodology used to obtain local concentration from the local Raman spectra has been described previously.[27] It takes about 20 min to acquire the whole concentration profile. The operative depth resolution in the instrumental conditions of the present work (λ = 632.8 nm, NA = 1.39, h = 200 μm) was obtained by scanning in z-direction the intensity of the 520 cm^{-1} band of a silicon wafer immersed in the coupling oil. Silicon acts as a layer of infinitesimal thickness, providing the point-by-point depth response of the instrument. The full width at half-maximum from the bell shaped curve (nominal depth resolution) that was obtained was 3.2 μm.

Results

Figure 2A−C shows representative liquid PS concentration profiles for diffusion experiments conducted at temperatures well below the T_g of the corresponding glassy matrices. Figure 2A shows the volume fraction of PS (Φ^{PS}) for the l-PS0.7/g-PPO interphase, which was annealed at 140 °C (60 °C below the matrix T_g), for several time lengths. Figure 2B,C shows the same information for the l-PS1.5/g-PPO and l-PS0.7/g-PPO interphases, held at 160 and 180 °C, respectively, about 20 °C below the corresponding matrix T_g. To obtain these concentration profiles, "optical sectioning" by confocal Raman was started at the rich-PPO/coupling oil interface, the zero in the depth scale axis, and then repeated at deeper positions along the PPO diffusion path.

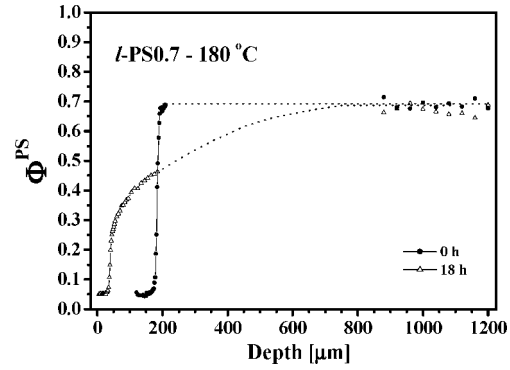

Figure 3. Complete PS profile showing the range of depths covered by confocal Raman measurements. Dotted lines were drawn as a guide to the eye.

Overall, the profiles shown in Figure 2 look sharper and better defined than those reported in earlier work, which reflects the substantial improvement in depth resolution obtained by working within the diffraction limit instead of limited by refraction.[28] Originally, the boundary between polymer layers was located at about 200 μm on the depth scale, dividing glassy (0−200 μm) and liquid (200−1200 μm) regions. As time increased, PS advanced toward the PPO-rich side in the form of sharp diffusion fronts. Behind the fronts, the profiles are fairly flat, with subtle differences depending on PS molecular weight and temperature. Notice that the experiment captures the profile region within the working distance of the microscope objective (210 μm) and that a major part of the liquid layer is beyond the observational window. The original thickness of this layer was set to about 1000 μm to satisfy the condition of infinite liquid supply, i.e., l-PS diffusion from a source of invariant properties. This condition was verified by placing the composite specimen upside-down on the microscope stage and using a "dry" objective to examine changes from the outside of the PS-rich layer. An example of this type of data is given in Figure 3, which shows experimental information obtained with both types of objectives. Data correspond to the l-PS0.7/g-PPO system, before and after being annealed for 18 h at 180 °C. Data in the range of depths between 0 and 200 μm are the same that those shown in Figure 2C, while data in the range 850−1200 μm were obtained with a dry objective. We see that PS concentration on the right border of the polymer couple did not deplete with diffusion time, remaining essentially constant. This verifies that the liquid is supplied from a plasticized layer that remains invariant in concentration, which is different from previous studies on this system, where polymer liquid concentration in the plasticized layer was found to considerably decrease in the course of the diffusion process.[12,19]

Figures 4 and 5 present a series of plots that characterize the interphase kinetics in the PS/PPO polymer pair. We mainly focus on the time evolution of front positions, a direct way of revealing the type of scaling for the diffusion controlling step. With a depth resolution of about 3 μm, invariant with focusing depth, the localization of the diffusion front is now straightforward and precise. Indirect calculations employed in previous work, arising from the lower depth resolution of the focusing mode employed, were not needed.[28] The position of the diffusion front was calculated as the maximum of the derivative curve of the PS concentration profile. In Figure 4, the aim is to explore

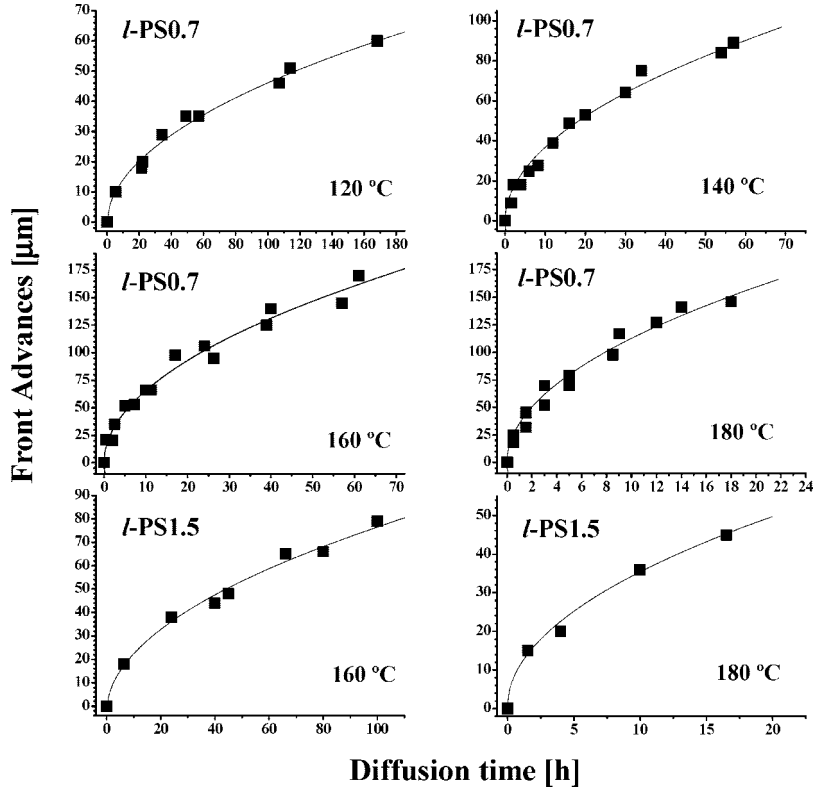

Figure 4. Kinetics of the advancing diffusion front as a function of the elapsed diffusion time for several diffusion temperature, for two of the PS samples (*l*-PS0.7 and *l*-PS1.5).

the advancing diffusion front positions in the context of the case II diffusion theory, showing the successive front positions as a function of annealing time. Figure 5 shows the same plot in the Fickean fashion as a function of the square root of the elapsed diffusion time.

Discussion

Analysis of Diffusion Kinetics. We begin by examining details of the shape of the liquid diffusion profiles. Overall, they show a marked asymmetry, ascribed to the dramatic changes in molecular mobility experienced by the PS chains in the pathway from the liquid to the glassy side. As a common feature for all the experiments, the profile in the liquid−glassy transition region drops off sharply, in a form of diffusion front. The steep front is a result of the beginning of the high-T_g region (low PS content), where molecular mobility decreases dramatically. On the scale of the spatial discrimination of our experimental technique, the diffusion fronts are sharp, with no leading tails: the rounding observed at the profiles' edges entering to the glassy layer has a width on the order of the depth resolution of the technique.

Throughout the liquid layer (high PS content region), which is highly plasticized at the temperature of the experiment, the volume fraction of PS is fairly constant, indicating that, once incorporated to this layer, distribution of PPO molecules is rapid. Depending on PS molecular weight and temperature, we observe differences in the local slope of the liquid profiles and a shifting in the PS volume fraction where profiles crossover (see Figure 2). As this region is in the liquid state at the temperature of the experiment, these differences can be explained in terms of the particular T_g of each PS sample, which at the end affects the composition dependence of chain diffusivity.

In the context of the diffusion mechanisms under discussion, the presence of sharp diffusion fronts followed by a highly plasticized region with nearly constant liquid concentration appears at first sight compatible with both Fickean and case II mechanisms. Both Fickean diffusion models with variable (locally adjusted) D values and classic case II treatments give rise to liquid profiles with the above-mentioned characteristics. There is, however, a typical case II feature apparently absent: the Fickean concentration tails preceding the advancing front. Fickean tails develop over the so-called induction period and persist as precursors of the advancing case II front. They form by random movements of the small molecules through interstitial sites in the glassy polymer (free volume) and play an important role in plasticizing the glassy matrix, additionally reducing its yield stress and thus favoring case II initiation. Typically, Fickean tails extend over ranges of several hundreds of nanometers[2b] and one may argue that, if present, they are overlooked by CRM. It will be shortly shown that, when the interphase is examined at higher spatial resolution, concentration tails are truly absent in this type of system. We have advanced some reasons for this apparent common pattern: the probability that local fluctuations in density produce a hole of sufficient size for a large-sized molecule to move in the glassy matrix is very small.[19]

Solid evidence to discern the nature of the rate-controlling step for liquid transport can be obtained from the analysis of the time scaling laws for the diffusion front propagation revealed by Figures 4 and 5. Figure 4 shows that for all our experiments the displacements of the PS diffusion fronts that advance into the glassy matrix are markedly nonlinear with time. At this point, we should consider that the experimental setup guarantees diffusion under almost constant liquid supply over the complete process and that this condition necessarily leads to the observation of linear diffusion kinetics in case II conditions. Thus, the marked departure from a linear front advance−time relationship definitively rules out the occurrence of case II in our experiments. On the contrary, the very close scaling of front advances with $t^{1/2}$ observed in Figure 5 strongly suggests that the transport of PPO toward the PS layer is Fickean in all of the cases. The obedience to a $t^{1/2}$ scaling law is remarkable given the large

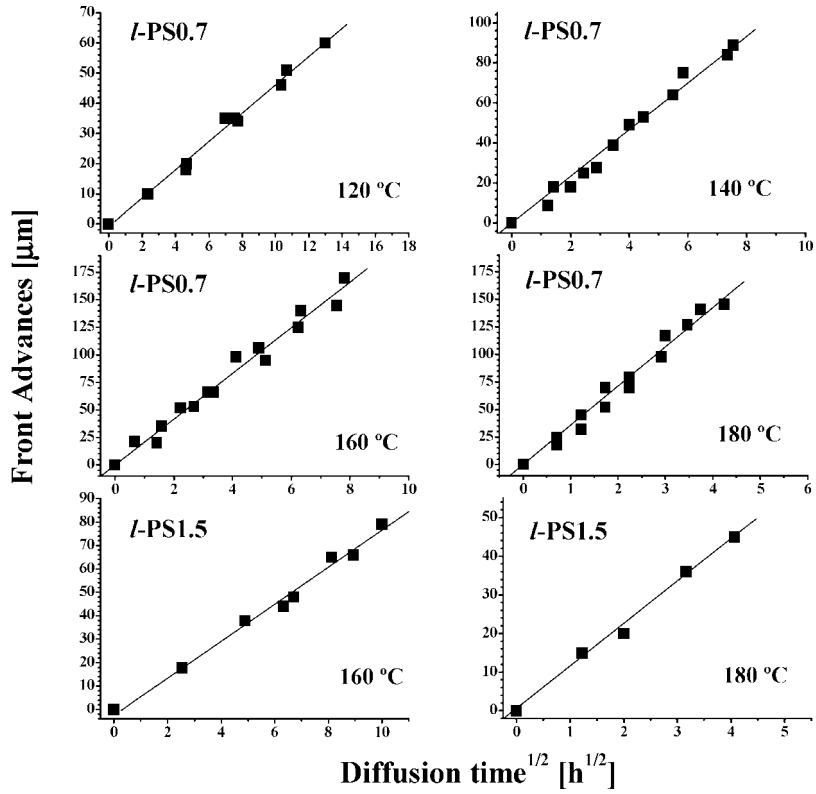

Figure 5. Advancing diffusion front kinetics plotted in Fickean fashion for several diffusion temperatures and two of the PS samples studied.

amount of experimental data collected, which includes several PS samples with molecular weights in the lower end, and wide ranges of annealing time and temperatures. Notice the absence of departures from linearity typically observed in previous experiments carried out under conditions of limited liquid supply.[19]

Comparison with Other Diffusion Experiments in the l-PS/g-PPO System. The first experiments on the l-PS/g-PPO system were reported by Composto et al.[6] They studied the diffusion of PS (M_w = 390 kg/mol) into a pure PPO matrix (M_w = 35 kg/mol) at temperatures between 6 and 39 °C below the PPO T_g, using Rutherford backscattering spectrometry (RBS). Diffusion was promoted through a planar interface between a 2 μm thick PS layer with a 1 μm thick layer of pure PPO on top. The authors reported PPO profiles with a marked asymmetry, complementary to those reported here for the PS species: a steep slope or diffusion front at high PPO volume fractions, followed by a rather flat region at higher depths, where PPO concentration is much lower and almost uniform. The diffusion fronts were sharp, with no indication of preceding concentration tails. This point is relevant, as discussed earlier, given the excellent depth resolution of the technique employed, which is able to resolve diffusion distances below 30 nm. The authors observed that the displacement of the interface followed a $t^{1/2}$ scaling law. A close inspection of the data (Figure 8, ref 6) reveals that the plots are not strictly linear and show the same type of downward curvature observed in limited liquid supply experiments.[19] The Matano−Boltzmann analysis applied to the data showed that the diffusion coefficients extracted from concentration profiles were in good agreement with those predicted by diffusion theories for polymer dynamics in the melt state. Overall, these results appear fully compatible with the Fickean case, showing no evidence of case II.

In contradiction with these observations, Lin and co-workers recently claimed evidence of case II in a new set of diffusion experiments monitored by secondary ion mass spectroscopy (SIMS). The molecular weight of the PPO sample used was M_w = 244 kg/mol (M_w/M_n = 3); the PS samples, nearly monodisperse, had molecular weights ranging from 9 up to 2000 kg/mol. Diffusion samples consisted of a flat 0.5 μm thick PS layer deposited on top of a 0.5 μm thick PPO layer, which were subsequently annealed at temperatures well below the PPO T_g. Via SIMS, the authors were able to probe the l-PS/g-PPO interphase with a spatial (depth) resolution of 10 nm. The PPO concentration profiles reported were not symmetric, showing similar features to those reported here and previously by Composto. Confirming what appears as a common feature in these systems, the diffusion fronts reported look remarkably steep at a resolution of 10 nm, with no discernible tails in front. As the thickness of both PS and PPO layers were comparable, marked effects of the limited PS supply were observed. For instance, the average Φ^{PS} throughout the liquid layer decreases from 1 to 0.7 in the course of the experiment (see Figure 2, ref 12). Although the PPO concentration profiles shown are remarkably clear, reported data on diffusion kinetics were relatively scarce, with at most four experimental data (front advances) in each example shown (only two). The analysis of the diffusion kinetics is not conclusive: while some of the data show an apparently linear tendency, others show a clear Fickean dependence.

Using the argument of the marked asymmetry of the liquid concentration profile, Lin claims that the liquid−glassy polymer interphase evolves via a case II mechanism. To explain such evolution, the authors envision the existence of an "intermixing layer", whose width is determined by two arbitrarily positioned planes (see Figure 5, ref 12). One of those planes limits the pure glassy PPO layer; the second one is positioned where the PPO−PS interphase becomes liquid during the annealing that promotes diffusion. The authors determined the position of the second plane by calculating local T_g values from the measured PPO concentration profile via Flory−Fox equation. In other words, the intermixing layer corresponds to the region

where the PPO−PS interphase remains glassy during the annealing process that promotes diffusion. Values of the intermixing layer thicknesses reported are in the range between 27 and 34 nm and change very little with PS molecular weight, despite the wide range covered (9200 and 2000 kg/mol). The authors propose that diffusion proceeds via case II diffusion in the intermixing layer but in normal Fickean fashion at the liquid side of the interphase.

Molecular Transport at the Liquid/Glassy Polymer Boundary. Our results on the l-PS/g-PPO diffusion indicate that the kinetics of liquid fronts advances in conditions of unlimited supply are clearly Fickean. Before proposing a mechanism that explains the observed behavior at the molecular level, we would like to offer a different interpretation of the valuable experimental data on the l-PS/g-PPO published by Lin. Our first point of disagreement is that the asymmetry of the liquid profiles is not itself a conclusive proof for case II, an argument used by many authors, including Lin. Unfortunately, the results on diffusion kinetics reported by Lin are not so extensive to discern between linear and square root time dependences due to the relatively narrow range of diffusion times studied. Besides, diffusion experiments were conducted in conditions of limited liquid supply and under continuous depletion of liquid PS concentration in the plasticized layer; in this configuration, scaling laws for diffusion kinetics have to be interpreted with caution, as discussed earlier. Therefore, from the point of view of the analysis of diffusion kinetics, we believe that there are no solid proofs for case II in Lin's results.

We share with the authors the idea of existence of an "intermixing layer", a region where those mass transport steps which are crucial to explain the overall diffusion kinetics take place. We disagree, however, on how this region is calculated and interpreted. On one hand, the assignment of local T_g values by calculation from a standard Flory−Fox equation may not be readily applicable to the PPO−PS interphase, as this equation is only valid for mixtures that can be considered homogeneous over length scales much larger than the average end-to-end distances for the polymer chains present. Considering that the average end-to-end distance for the PPO used is about 36 nm (see below), similar to the reported values for the intermixing layer thickness (about 30 nm), we see that the requisite is not fulfilled. On the other hand, Lin uses these local T_g values to somewhat define a limit for chain segment mobility that give rise to diffusion or not. The situation may not be so simple if self-concentration effects are considered, an idea proposed by Lodge and McLeish.[29] The Lodge−McLeish model predicts that, in homogeneous mixtures between polymers with widely different T_g, each component "feels" in the blend an environment enriched in itself, compared with the average blend composition. While the component with lower T_g can have a significant segmental mobility at temperatures quite lower than that predicted by Flory−Fox, the higher T_g component is characterized by the opposite. This conception has been shown to describe very well several aspects of the behavior of miscible blends, yielding a more accurate description of polymer dynamics at the monomeric level.[30] We found that by using the Lodge−McLeish model instead of the simple Fox−Flory equation the thickness values predicted for the intermixing layer were about 12−14 nm smaller (about 30−40%) than those reported in Figure 7 of ref 12. Again, the Lodge−McLeish approach applies to mixtures that are homogeneous for length scales much larger than the average end-to-end distances: for the large PS concentration gradients existing at the intermixing layer the differences with the Fox−Flory approach can be even more pronounced. Lin's too simple interpretation of T_g at short length scales may also have led to the author to claim the phenomenon of *glassy−glassy* polymer diffusion (Figure 10, ref 12), entirely based on calculating local T_gs from the simple Fox−Flory approach.

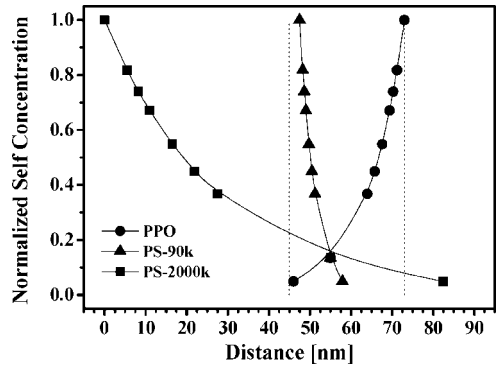

Figure 6. Normalized self-concentration profile for PS and PPO molecules, as calculated from their Gaussian autocorrelation functions.

It is useful to put values of intermixing layer thicknesses in context by comparing them with statistical parameters for the polymer molecules employed by Lin. For instance, the unperturbed end-to-end distance for PPO of $M_w = 200$ kg/mol is estimated to be at least 36 nm;[31] for PS samples of $M_w = 90$ kg/mol and $M_w = 2000$ kg/mol, referred to as PS-90K and PS-2000K, we calculated distances of 15 and 110 nm, respectively.[32] Figure 6 shows a sketch with normalized self-concentration profiles for individual chains of these three polymers, calculated from Gaussian autocorrelation functions.[32] For the depicted PPO concentration profiles the T_g of the pure liquid PS phase would be about 100 °C. The dotted vertical lines limit the thickness of the intermixing layer, calculated by averaging values of Lin's calculation and our estimation using the Lodge−McLeish model, and have been arbitrarily placed next to the PPO center of mass. The PS-2000K concentration is assumed to be essentially zero at the pure PPO glassy intermixing layer limit, as shown by Lin's experimental data. The position for the normalized PS-90K self-concentration profile was arbitrarily chosen with the center of mass of the molecule next to the intermixing layer of the liquid−glassy boundary.

As shown in this quantitative scale, the *whole* PPO concentration gradient, as measured in Lin experiments, develops over a length comparable with the end-to-end distance for an average PPO molecule. The dimensions of this region do not appear to be related with the end-to-end distance of the PS molecules, widely different for the set of liquid PS counterparts employed. These observations suggest that the dimension of the liquid−glassy boundary, from which originates the PPO molecules that diffuse toward the liquid side, is most likely controlled by the PPO end-to-end distance. The experimental work needed to confirm this idea requires looking for changes in the thickness of the intermixing layer in diffusion experiments with several PPO molecular weights and a given PS sample.

Lin's observation of the liquid−glassy boundary at length scales comparable with single chain dimensions gives us a deeper insight into the transport process at the molecular level. On the basis of Lin's results and our previous analysis, we now understand that PPO transport from the glassy side occurs as a sequence of events that start when *sections* of the PS molecules plasticize first the PPO molecules at the PPO−PS interface, almost one PPO molecule at a time, by short-range Rouse-like movements. These short scale displacements occur over length scales much smaller than the PPO end-to-end distance and do not involve center-of-mass displacements of PS chains. We believe that this process is favored by the experimental evidence that shows that, in the PS−PPO mixture, PS molecular segments

may display short-range movements at temperatures quite lower than the PPO molecules.[29] Once plasticized, the PPO molecules can diffuse in the liquid state toward the PS-rich liquid layer by a regular Fickean mechanism. The lack of support for a molecular mechanism initiated by Fickean penetration of the liquid followed by deformation of the glassy matrix, i.e., case II, arises from the complete absence of center-of-mass displacements observed for the PS chains toward the glassy side. As we proposed in our original work, we believe that these ideas are general and not particular to this polymer pair.

Conclusions

We have shown that the transport mechanism of l-PS into g-PPO when the PS source was unlimited was clearly Fickean. In a setting of unlimited supply of the liquid polymer, diffusion kinetics should be strictly linear if case II was operative; on the contrary, no manifestations of this diffusion mechanism were found. This behavior, documented in extensive ranges of annealing times and temperatures, refutes earlier reports on case II occurrence in this system. The mechanism of interphase evolution proposed embraces not only our experiments, carried out at microscopic level, but also previous observations of interphase evolution at level of single chain dimensions.

Although highly asymmetric liquid concentration profiles are commonly observed in diffusion experiments that involve a polymer matrix that remains glassy at the temperature of the experiment, we emphasize here that these are not *sufficient* conditions for case II occurrence. The fundamentals established by Thomas and Windle for case II diffusion define some essential conditions that should not be overlooked. We have discussed that the observation of strictly linear kinetics in case II diffusion is bounded to the condition of unlimited liquid supply. A close inspection of most of the liquid/glassy polymer diffusion experiments shows that this condition is frequently not met. A mechanism controlled by mechanical deformation of the solid matrix requires that penetrants generate high levels of osmotic suction, comparable to the yield stress of the solid matrix. This is definitively not the case for large liquid polymers employed in most of the previous studies, which generate osmotic suction levels orders of magnitude lower than those associated with small sized penetrants, such as, for instance, the methanol molecule utilized by Thomas and Windle in their studies of case II diffusion on poly(methyl methacrylate).[28] Finally, the response of case II to temperature and to the previous thermal history of the solid matrix is distinctive and markedly different to the Fickean case.[3] All these manifestations, and not only the phenomenology reflected in the shape of the diffusion profiles, have to be properly analyzed when diffusion mechanisms are investigated.

Acknowledgment. Financial support from ANPCYT (PICT 06-1359 and PICT 12-14570) and from AECID (A6060/06) made this research work possible. We thank Robert Roller for proofreading the manuscript.

References and Notes

(1) (a) Hui, C.-Y.; Wu, K.-C.; Lasky, R. C.; Kramer, E. J. *J. Appl. Phys.* **1987**, *61*, 5129. (b) Hui, C.-Y.; Wu, K.-C.; Lasky, R. C.; Kramer, E. J. *J. Appl. Phys.* **1987**, *61*, 5137.
(2) (a) Lasky, R. C.; Kramer, E. J.; Hui, C.-Y. *Polymer* **1988**, *29*, 673. (b) Gall, T. P.; Lasky, R. C.; Kramer, E. J. *Polymer* **1990**, *31*, 1491. (c) Gall, T. P.; Kramer, E. J. *Polymer* **1991**, *32*, 265.
(3) (a) Thomas, N. L.; Windle, A. H. *Polymer* **1980**, *21*, 613. (b) Thomas, N. L.; Windle, A. H. *Polymer* **1981**, *22*, 627. (c) Thomas, N. L.; Windle, A. H. *Polymer* **1982**, *23*, 529.
(4) Argon, A. S.; Cohen, R. E.; Patel, A. C. *Polymer* **1999**, *40*, 6991.
(5) In ref 4, Argon defines osmotic suction (Σ) using the context of thermodynamics of osmosis as the "driving force" for liquid penetration: $\Sigma = (kT/\Omega)\ \ln(\Phi_{eq}/\Phi)$, where Ω is the molar volume of the penetrant molecule, Φ is the concentration of penetrant at a given place, and Φ_{eq} is its temperature-dependent value at equilibrium.
(6) Composto, R. J.; Kramer, E. J. *J. Mater. Sci.* **1991**, *26*, 2815.
(7) Sauer, B. B.; Walsh, D. J. *Macromolecules* **1991**, *24*, 5948.
(8) Jabbari, E.; Peppas, N. A. *Macromolecules* **1993**, *26*, 6229.
(9) Tomba, J. P.; Carella, J. M.; García, D.; Pastor, J. M. *Macromolecules* **2001**, *34*, 2277.
(10) Geoghegan, M.; Jones, R. A. L.; Van der Grinten, M. G. D.; Clough, A. S. *Polymer* **1999**, *40*, 2323.
(11) Arzondo, L.; Tomba, J. P.; Carella, J. M.; Pastor, J. M. *Macromol. Rapid Commun.* **2005**, *26*, 632.
(12) Lin, C. J.; Tsai, I. F.; Yang, C. M.; Hsu, M. S.; Ling, Y. C. *Macromolecules* **2003**, *36*, 2464.
(13) Nealey, P. F.; Cohen, R. E.; Argon, A. S. *Polymer* **1995**, *36*, 3687.
(14) Wool, R. P. *Polymer Interfaces*; Hansen Publishers: Munich, 1995.
(15) (a) Doi, M.; Edwards, S. F. *The Theory of Polymer Dynamics*; Oxford University Press: Oxford, England, 1986. (b) de Gennes, P. G. *Scaling Concepts in Polymer Physics*; Cornell University Press: Ithaca, NY, 1979.
(16) (a) Kramer, E. J.; Green, P. F.; Palmstrom, C. J. *Polymer* **1984**, *25*, 473. (b) Composto, R. J.; Kramer, E. J.; White, D. M. *Macromolecules* **1988**, *21*, 2580.
(17) Tomba, J. P.; Carella, J. M. *J. Polym. Sci., Polym. Phys. Ed.* **1999**, *37*, 3097.
(18) Crank, J. *The Mathematics of Diffusion*; Clarendon: Oxford, United Kingdom, 1974.
(19) Tomba, J. P.; Arzondo, L.; Carella, J. M.; Pastor, J. M. *Macromol. Chem. Phys.* **2007**, *208*, 1110.
(20) Odrobina, E.; Winnik, M. A. *Macromolecules* **2001**, *34*, 6029.
(21) De Luca, A. C.; Rusciano, G.; Pesce, G.; Caserta, S.; Guido, S.; Sasso, A. *Macromolecules* **2008**, *41*, 5512.
(22) (a) Everall, N. *Appl. Spectrosc.* **2000**, *54*, 773. (b) Everall, N. *Appl. Spectrosc.* **2000**, *54*, 1515.
(23) Baldwin, K. J.; Batchelder, D. N. *Appl. Spectrosc.* **2001**, *55*, 517.
(24) Tomba, J. P.; Arzondo, L. M.; Pastor, J. M. *Appl. Spectrosc.* **2007**, *61*, 177.
(25) Tomba, J. P.; Carella, J. M.; Pastor, J. M.; Merino, J. C. *Polymer* **2002**, *43*, 6751.
(26) Tomba, J. P.; Pastor, J. M. *Macromol. Chem. Phys.* **2009**, *210*, 549.
(27) Tomba, J. P.; De la Puente, E.; Pastor, J. M. *J. Polym. Sci., Part B: Polym. Phys.* **2000**, *38*, 1013.
(28) Tomba, J. P.; Carella, J. M.; Pastor, J. M. *Macromolecules* **2005**, *38*, 4355.
(29) Lodge, T. P.; McLeish, T. C. B. *Macromolecules* **2000**, *33*, 5278.
(30) (a) Leroy, E.; Alegría, A.; Colmenero, J. *Macromolecules* **2002**, *35*, 5587. (b) Sakaguchi, T.; Taniguchi, N.; Urakawa, O.; Adachi, K. *Macromolecules* **2005**, *38*, 4355.
(31) (a) Akers, P. J.; Allen, G.; Bethell, M. J. *Polymer* **1968**, *9*, 575. (b) Barrales-Rienda, J. M.; Pepper, D. C. *Polym. Lett.* **1956**, *4*, 959.
(32) Flory, P. J. *Statistical Mechanics of Chain Molecules*; J. Wiley & Sons: New York, 1969.

MA802884J